

2021

Comprehensive Collagen Crosslinking Comparison of Microfluidic Wet-Extruded Microfibers for Bioactive Surgical Suture Development

Amrita Dasgupta

Nardos Sori

Stella Petrova

Yas Maghdouri-White

Nick Thayer

See next page for additional authors

Follow this and additional works at: https://digitalcommons.odu.edu/bioelectrics_pubs



Part of the [Biomedical Commons](#), and the [Musculoskeletal System Commons](#)

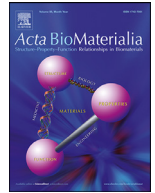
Original Publication Citation

Dasgupta, A., Sori, N., Petrova, S., Maghdouri-White, Y., Thayer, N., Kemper, N., Polk, S., Leathers, D., Coughenour, K., Dascoli, J., Palikonda, R., Donahue, C., Bulysheva, A. A., & Francis, M. P. (2021). Comprehensive collagen crosslinking comparison of microfluidic wet-extruded microfibers for bioactive surgical suture development. *Acta Biomaterialia*, 128, 186-200. <https://doi.org/10.1016/j.actbio.2021.04.028>

This Article is brought to you for free and open access by the Frank Reidy Research Center for Bioelectrics at ODU Digital Commons. It has been accepted for inclusion in Bioelectrics Publications by an authorized administrator of ODU Digital Commons. For more information, please contact digitalcommons@odu.edu.

Authors

Amrita Dasgupta, Nardos Sori, Stella Petrova, Yas Maghdouri-White, Nick Thayer, Nathan Kemper, Seth Polk, Delaney Leathers, Kelly Coughenour, Jake Dascoli, Riya Palikonda, Connor Donahue, Anna A. Bulysheva, and Michael P. Francis



Full length article

Comprehensive collagen crosslinking comparison of microfluidic wet-extruded microfibers for bioactive surgical suture development



Amrita Dasgupta^a, Nardos Sori^a, Stella Petrova^a, Yas Maghdouri-White^a, Nick Thayer^a, Nathan Kemper^a, Seth Polk^a, Delaney Leathers^{a,b}, Kelly Coughenour^a, Jake Dascoli^a, Riya Palikonda^c, Connor Donahue^a, Anna A. Bulysheva^d, Michael P. Francis^{a,b,*}

^a Embody Inc., Norfolk, VA 23508, United States

^b Eastern Virginia Medical School, Norfolk, VA 23507, United States

^c Virginia Commonwealth University, Richmond, VA 22908, United States

^d Old Dominion University, Norfolk, VA 23508, United States

ARTICLE INFO

Article history:

Received 23 February 2021

Revised 13 April 2021

Accepted 13 April 2021

Available online 19 April 2021

Keywords:

Collagen

Microfiber

Microfluidic wet-extrusion

Crosslinking

Suture

Bioactive

Internal brace

Biotextile

Smart fiber

Smart fabric

BioRegenerative

Sports medicine

ABSTRACT

Collagen microfiber-based constructs have garnered considerable attention for ligament, tendon, and other soft tissue repairs, yet with limited clinical translation due to strength, biocompatibility, scalable manufacturing, and other challenges. Crosslinking collagen fibers improves mechanical properties; however, questions remain regarding optimal crosslinking chemistries, biocompatibility, biodegradation, long-term stability, and potential for biotextile assemble at scale, limiting their clinical usefulness. Here, we assessed over 50 different crosslinking chemistries on microfluidic wet-extruded collagen microfibers made with clinically relevant collagen to optimize collagen fibers as a biotextile yarn for suture or other medical device manufacture. The endogenous collagen crosslinker, glyoxal, provides extraordinary fiber ultimate tensile strength near 300MPa, and Young's modulus of over 3GPa while retaining 50% of the initial load-bearing capacity through 6 months as hydrated. Glyoxal crosslinked collagen fibers further proved cytocompatible and biocompatible per ISO 10993-based testing, and further elicits a predominantly M2 macrophage response. Remarkably these strong collagen fibers are amenable to industrial braiding to form strong collagen fiber sutures. Collagen microfluidic wet extrusion with glyoxal crosslinking thus progress bioengineered, strong, and stable collagen microfibers significantly towards clinical use for potentially promoting efficient healing compared to existing suture materials.

Statement of Significance

Towards improving clinical outcomes for over 1 million ligament and tendon surgeries performed annually, we report an advanced microfluidic extrusion process for type I collagen microfiber manufacturing for biological suture and other biotextile manufacturing. This manuscript reports the most extensive wet-extruded collagen fiber crosslinking compendium published to date, providing a tremendous recourse to the field. Collagen fibers made with clinical-grade collagen and crosslinked with glyoxal, exhibit tensile strength and stability that surpasses all prior reports. This is the first report demonstrating that glyoxal, a native tissue crosslinker, has the extraordinary ability to produce strong, cytocompatible, and biocompatible collagen microfibers. These collagen microfibers are ideal for advanced research and clinical use as surgical suture or other tissue-engineered medical products for sports medicine, orthopedics, and other surgical indications.

© 2021 The Author(s). Published by Elsevier Ltd on behalf of Acta Materialia Inc.

This is an open access article under the CC BY-NC-ND license

(<http://creativecommons.org/licenses/by-nc-nd/4.0/>)

* Corresponding author at: 4211 Monarch Way STE 500, Norfolk, VA 23508, United States

E-mail addresses: mfrancis@embody-inc.com, mpf3b@virginia.edu (M.P. Francis).

1. Introduction

Regarding ligament and tendon repairs for the extremities, in the US, around 800,000 shoulder repairs, 300,000 foot and ankle repairs, and 200,000 knee surgical soft tissue repairs are performed annually [1–4], all involving sutures. Surgical interventions to augment, repair, or reconstruct tendons and ligaments include autografts, allografts, and synthetic materials as sutures, braces, or grafts for soft tissue closure or joining [5,6], each with clinical limitations. Allografts can be slow to integrate, inflammatory, and may delay healing [4,7,8]. Synthetic grafts or sutures (or “internal braces”) elicit a foreign body immune response and can break down into acidic byproducts damaging surrounding tissue [9–11]. Synthetic sutures often do not match the mechanical or material properties of tendons or ligaments [12], which may lead to the generation of stress risers and the creation of a debilitating non-isometry if used in a joint space. Autografting extends surgery time and associated trauma (e.g., blood loss, risk of infection) due to the need for a second procedure to recover the autologous tissue [3,13]. Joint reconstruction with autografting or allografting further results in a higher incidence and severity of premature osteoarthritis, affecting the patients’ quality of life [3,14–16].

The opportunity to improve clinical outcomes from current connective tissue reconstruction strategies has led to the emergence of innovative tissue engineering approaches. These approaches aim to develop biocompatible materials that can remodel *in vivo* and subsequently be biologically integrated by *in situ* tissue remodeling, thus regenerating typical anatomical structure with restored mechanical strength [17,18].

Structural and biomechanical functionality in tendons and ligaments is attributed primarily to the presence of dense, aligned fibrillar type I collagen [2,4,19,20]. Therefore, several efforts in generating biomaterials to support connective tissue repair have incorporated collagen [3,21–23]. Type I collagen in the form of a lyophilized sponge was successful in early-stage testing for ACL repair in a porcine model [24], where collagen proved a beneficial porous regenerative matrix [25–28]. However, the need for an open surgical procedure and the inability for the mechanically deficient collagen sponge to restore initial mechanical strength has led to exploring alternatives for regenerative rehabilitation of ligament, tendon, and other soft tissue repairs.

Collagen-based biomaterials have garnered considerable attention in numerous other applications such as sutures for wound closure, hemostasis, hernia repair, repair of bone and cartilage defects, and treatment of burns [29–31]. Sutures are integral to efficient wound healing. However, there is still an unmet need in additive manufacturing for a biological and strong suture. Collagen, with its vital role in wound healing [32], may address such an ideal. Historically for collagen-based sutures, catgut resorbable sutures (plain or chromic) have been used in wound healing [33–35]. Tissue reactivity, rapid loss in tensile strength, and unpredictable resorption rates have restricted chromium crosslinked catgut suture applications [36]. Collagen-coated synthetic suture fibers (e.g., Collagen-Coated FiberWire®) are available, yet without claims for enhancing or bioactivity.

Type I collagen can be additively manufactured by extrusion into fibers [37,38] which exhibit an increase in mechanical strength when crosslinked [39–41]. However, most crosslinkers are cytotoxic and use chemicals foreign and toxic to the body. Furthermore, prior work on collagen wet-extrusion uses collagen from sources not extracted under current good manufacturing practices (GMP) conditions and thus not suited for medical device manufacturing, complicating these studies’ clinical relevance [39,40,42–45].

This study develops a high output microfluidic wet-extrusion system to produce consistent and scalable microfibers of clinically relevant type I collagen as filaments and thin ribbon-like struc-

tures. We optimized fiber production techniques, tested over 50 different crosslinking formulations, and performed rigorous mechanical and biochemical tests to optimize fundamental fiber properties specifically for biomedical use. These collagen fibers have potential applications in tendon and ligament repair, wound closure, and other indications where an advanced collagen-suture-based biomaterial may be beneficial across the fields of surgery in medicine.

2. Materials and methods

2.1. Collagen preparation and fiber production

2% (w/v) clinical grade lyophilized telocollagen (Telo) or atelocollagen (Atelo) was used from Collagen Solutions(CA) or as research-grade methacrylated collagen (Advanced BioMatrix, CA) was used in these studies. Collagen was dissolved in 0.05 M acetic acid or 0.01M hydrochloric acid overnight by agitation. Acidified collagen was then pumped through the center of a coaxially arranged set of needles (inner diameter of 0.4mm) at a flow rate of 0.06ml/min (setup shown in supplementary Fig. S1). A neutralizing alkaline formation phosphate buffer containing salts (at pH 8) (Sodium chloride, Sodium Phosphate Dibasic, Sodium Phosphate Monobasic, and N-Tris(hydroxymethyl)methyl-2-aminoethanesulfonic acid) and PEG (polyethylene glycol) were pumped through the outer portion of the coaxial needle and into a formation tube of length 610mm. The collagen solution emerged into the center of the formation tube. The formation buffer ran at a volumetric flow rate ten times higher than the collagen, which caused the protein extension and alignment, imparting mechanical strength to the resulting fiber. The fiber became more solid as it passed through the formation tube (dwell time of up to 1.5 minutes) before entering a bath of 20% aqueous ethanol. In addition to dehydrating the fiber, this bath helped remove residual formation buffer, thus contributing to improved strength and stability of the resultant collagen microfiber. After dehydration, the microfiber was collected on a two-bar device or the solid spool. Collected microfibers were air-dried for a half hour and subsequently crosslinked under different experimental conditions. Chemical reagents used during extrusion and crosslinking are included in Supplementary Table S1.

2.2. Microfiber crosslinking

In situ crosslinking (chemical or enzymatic) for the groups shown in Table 1 was performed by dissolving the determined amount of the crosslinker in acidified collagen mixture for the time stated in Table 1. Microfibers from *in situ* crosslinked collagen were then extruded onto a two-bar device and kept taut, as shown in Fig. S2.

Post-extrusion chemical crosslinking, untreated or *in situ* crosslinked, and taut collagen microfibers extruded on the two-bar device or the solid spools were air-dried a half hour and then submerged into a solution of crosslinker in 70% ethanol solution and then placed on a rocker at low speed. Post crosslinking, microfibers were stored in a desiccator. Previous reports used to obtain information on various chemical crosslinkers, their concentrations, and crosslinking durations are provided in Table 1.

The DHT for crosslinking microfibers involved dehydrating relaxed extruded microfibers at 110°C and under vacuum for 1, 3, and 5 days with or without additional glyoxal crosslinking as described above.

For UVR mediated crosslinking, methacrylated collagen was used for extrusion. The extruded microfibers were exposed to a 365nm emitting UV light source for 20 minutes. These microfibers

Table 1

Collagen Microfiber Crosslinking Strength Comparison. Conditions highlighted in red were selected for further characterization post crosslinking optimization.

Crosslinker	Collagen Starting Material	In Situ	Post	Crosslinker Concentration	Time [hours]	Mean UTS [MPa] ± S.E.M.	References
Untreated	Telocollagen					6.1 ± 1.2	
Untreated	Atelocollagen					8.8 ± 1.7	
Choline Bitartrate	Telocollagen	Y		1mM	0.5	CBD ^a	[46]
Choline Bitartrate	Telocollagen	Y		100mM	0.5	CBD ^a	
Dehydrothermal treatment (DHT)	Telocollagen		Y		72	16.0 ± 1.2*	[47,48]
DHT	Telocollagen		Y		120	13.1 ± 0.7	
DHT	Telocollagen		Y		24	4.7 ± 0.4	
DHT/Glyoxal	Telocollagen		Y	10mM	120/24	27.2 ± 2.8*	[39,40]
DHT/Glyoxal	Telocollagen		Y	10mM	24/24	22.0 ± 3.0	
DL-Glyceraldehyde	Atelocollagen		Y	25mM	72	128.0 ± 11.8*	
DL-Glyceraldehyde	Telocollagen		Y	25mM	24	70.5 ± 6.0	
DL-Glyceraldehyde	Atelocollagen		Y	25mM	24	50.7 ± 3.3	
DL-Glyceraldehyde	Telocollagen		Y	25mM	72	40.3 ± 1.8	
DL-Glyceraldehyde	Telocollagen		Y	10mM	24	37.1 ± 2.2	
DL-Glyceraldehyde	Telocollagen		Y	5mM	24	35.3 ± 2.1	
DL-Glyceraldehyde	Telocollagen		Y	50mM	24	31.1 ± 1.2	
DL-Glyceraldehyde	Telocollagen	Y		250mM	5	27.3 ± 1.6	
DL-Glyceraldehyde	Telocollagen	Y		500mM	24	60.4 ± 1.5	
DL-Glyceraldehyde	Telocollagen		Y	250mM	5	60.2 ± 4.5	
DL-Glyceraldehyde	Telocollagen		Y	500mM	5	28.6 ± 1.5	
EDC	Telocollagen		Y	0.25mM	24	16.6 ± 1.5*	[42]
EDC	Telocollagen	Y		0.25mM	4	6.5 ± 0.5	
EDC	Telocollagen	Y		0.25mM	1	2.8 ± 0.1	
EDC/NHS	Telocollagen		Y	0.25mM/0.125mM	24	30.2 ± 1.0*	[49,50]
EGCG	Telocollagen	Y		200[μM]	2	2.2 ± 0.1*	[51]
EGCG	Telocollagen	Y		1mM	2	1.1 ± 0.1	
Glyoxal	Telocollagen		Y	10mM	72	121.2 ± 7.4*	[52]
Glyoxal	Telocollagen		Y	10mM	24	109.0 ± 7.4	
Glyoxal	Telocollagen		Y	100mM	72	76.2 ± 8.0	
Glyoxal	Atelocollagen		Y	10mM	24	62.1 ± 4.9	
Glyoxal	Telocollagen		Y	1mM	24	49.4 ± 1.6	
Glyoxal	Telocollagen		Y	5mM	24	45.9 ± 4.1	
Glyoxal	Atelocollagen		Y	10mM	72	28.6 ± 2.8	
Glyoxal	Telocollagen		Y	500mM	72	86.9 ± 5.5	
Glyoxal	Telocollagen		Y	0.5mM	24	48.3 ± 2.2	
Glyoxal	Telocollagen	Y		10mM	5	5.1 ± 0.2	
Glyoxal	Telocollagen	Y		0.5mM	5	2.3 ± 0.4	
Glyoxal/DHT	Telocollagen		Y	10mM	24/24	24.2 ± 1.3	
Glyoxal/Vegetable Oil	Telocollagen		Y	10mM	24/72	27.6 ± 2.2	
Liquid Transglutaminase/ Glyoxal	Telocollagen	Y	Y	0.1mg/ml 10mM	72	6.2 ± 1.0	
L-Lysine/Glyoxal	Telocollagen	Y	Y	10mM/10mM	2/24	96.9 ± 4.6*	
L-Lysine/Glyoxal	Telocollagen	Y	Y	5mM/10mM	2/24	32.2 ± 1.5	
Methyl Glyoxal	Telocollagen		Y	10mM	24	42.3 ± 4.1	
NDGA	Telocollagen		Y	0.01gm/ml	24	47.9 ± 4.2	[39,53]
O-Dextran	Telocollagen		Y	20% [w/v]	24	4.4 ± 0.1	
Procyanidin	Telocollagen		Y	2.5mg/ml	24	19.3 ± 1.5	
Procyanidin	Telocollagen		Y	5mg/ml	24	13.3 ± 0.9	
D-Sorbitol/Glyoxal	Telocollagen	Y	Y	330mM/10mM	72	22.2 ± 5.2	
D-Sorbitol	Telocollagen		Y	200mM	72	14.4 ± 0.7*	
D-Sorbitol	Telocollagen		Y	100mM	72	5.8 ± 0.4	
D-Sorbitol	Telocollagen	Y		200mM	5	1.9 ± 0.2	
UVR	Methacrylated		Y		0.3	1.9 ± 0.2	
UVR/Glyoxal	Methacrylated		Y	10mM	0.3/24	86.6 ± 10.1*	

^a CBD: Could not be determined;

* Significantly High UTS for the crosslinker group ($p < 0.01$)

were then placed in a desiccator or further crosslinked with 10mM glyoxal in 70% aqueous ethanol.

Optimization in manufacturing techniques led to a change in the microfiber collection method during extrusion. The two-bar setup was replaced by a solid spool (Supplementary Fig. S2) with closely spaced grooves, and microfibers were collected directly onto these grooves while maintaining tautness. In comparison to the two-bar device, collection onto spools helped scale up our microfiber production significantly. Spools of collagen microfibers were crosslinked using various chemicals in 70% aqueous ethanol

in acrylic tubes placed on rollers and rotated at 1 rpm to ensure uniform microfiber crosslinking.

2.3. Mechanical testing of collagen microfibers

To meet the demands of rigorous mechanical testing relevant to collagen microfibers' performance *in vivo*, we developed a high-throughput method of wet-tensile-testing microfiber samples (Supplementary Fig. S3). This method is described in detail in supplementary method S1.1.

2.4. Scanning electron microscopy (SEM)

SEM imaging was used to obtain cross-sectional and longitudinal microstructural signatures of our untreated/non-chemically cross-linked and cross-linked extruded microfibers. SEM imaging was performed at Embody, Inc. (Norfolk, VA) using a Zeiss Evo 10 microscope (Zeiss) with a 10kV beam intensity. For cross-sections, microfiber bundles were soaked in DPBS for 30 minutes, dried for an hour on SEM stubs, sputter-coated, and imaged.

2.5. Degree of crosslinking

We used ninhydrin assay to evaluate the number of free amino groups in glyoxal and DL-Glyceraldehyde crosslinked microfibers following the manufacturer's protocol (details in Supplemental Methods S1.3).

2.6. Differential scanning calorimetry (DSC) and Fourier-transform infrared (FTIR) spectroscopy of microfibers

DSC was performed using a Differential Scanning Calorimeter (DSC2500, TA Instruments, DE), and FTIR spectroscopy was performed on Platinum ATR (Bruker, Billerica, MA) at Old Dominion University (ODU) (Norfolk, VA). FTIR spectra were obtained from 400 cm^{-1} to 4000 cm^{-1} at a resolution of 4 cm^{-1} and averaged over 32 scans. Untreated and crosslinked microfibers were compared to the starting material by assessing shifts in peaks with the Essential FTIR bioinformatics software (Operant, Madison, WI).

2.7. Cell attachment, cytocompatibility, viability, and cytotoxicity assays

Crosslinked collagen microfibers were sealed inside Tyvek pouches with a STERRAD chemical indicator (4MD Medical Solutions, Lakewood, NJ) and sent for E-beam sterilization (Steri-Tek, Fremont, CA) using a 20kGy \pm 2kGy target dose.

Sterilized glyoxal and DL-Glyceraldehyde crosslinked microfibers were hydrated in tenocyte growth media (ZenBio, NC) for 30 minutes and placed in 24-well plates pre-coated with Poly (2-hydroxyethyl methacrylate) (pHEMA) (Sigma Aldrich) to inhibit cell binding to the culture vessel. Human tenocytes (ZenBio, NC) (in 100 μl tenocyte growth media) were seeded at 2.5×10^4 on sterilized microfibers in triplicates. After seeding, cells were allowed to attach for 1 hour before an additional 500 μl of tenocyte growth media was added. After 12 days in culture, tenocytes attached to collagen microfibers were stained with live cellular stain, CellTracker™ Green CMFDA (5-chloromethylfluorescein diacetate) (Thermo Fisher Scientific) following the manufacturer's protocol. Samples were then fixed using 4% paraformaldehyde and subsequently stained with a nuclear stain, DAPI (Thermo Fisher Scientific), to visualize attached tenocytes on microfibers using a confocal microscope (Zeiss Axio Observer Z1, Zeiss) at Eastern Virginia Medical School, Norfolk, VA.

Cytotoxicity from extruded microfibers effects on human tenocytes was assessed using the CyQuant Lactate Dehydrogenase (LDH) cytotoxicity assay kit (Invitrogen) and MTT (3-(4,5-dimethylthiazol-2-yl)-2,5-diphenyl tetrazolium bromide) assay kit (Sigma Aldrich) per manufacturer's protocol. After optimizing seeding density for the assay, 7×10^3 tenocytes were plated on each well of 48-well plates and allowed to grow for 24 hours in tenocyte growth media in a humidified incubator maintained at 37°C and 5% CO₂. Sterilized microfiber bundles were rinsed for 10 minutes in cell culture media and placed on tenocytes in each well. Tenocytes grown on plastic (cells only) were used as positive (for cell survival or viability) controls. Zinc dibutylthiocarbamate

(ZDBC) film and 10mM glyoxal were used as negative (for cell survival or viability) controls. The effects of Ethicon vicryl suture were also assessed as a control in this experiment as it was used to hold our extruded microfiber bundles together in early testing. Wells seeded with tenocytes and controls as described in the manufacturer's protocol. Samples were incubated for seven days before assessing the release of LDH in the media. Cytotoxicity per the LDH assay was calculated following the manufacturer's protocol, with cell survival percentage calculated as 100 - % cytotoxicity. Cell viability using MTT assay was calculated following the manufacturer's protocol.

The health and viability of live tenocytes growing with our extruded microfibers were additionally assessed using the AlamarBlue™ assay (Bio-Rad, Hercules, CA) as per the manufacturer's protocol.

2.8. Subcutaneous implants of crosslinked microfiber bundles in rats

According to an Institutional Animal Care and Use Committee (IACUC) approved protocol, all surgical procedures were conducted at Old Dominion University, Norfolk, VA. Per ISO 10993-6, n=6 crosslinked collagen microfiber bundles (prepared and sterilized as described in Section 4.8) and commercially available collagen-coated polyester, and ultrahigh molecular weight polyethylene (UHMWPE) suture (FiberWire™ from Arthrex, FL, in date from www.esuture.com) were implanted subcutaneously in female Sprague Dawley rats. Rats were anesthetized with isoflurane inhalation. Incisions were made dorsally in the flank area, and a hemostat was used to create a pocket for implants. After four weeks, the rats were humanely euthanized for tissue collection.

2.9. Histology

Harvested microfiber explants at four weeks were fixed in 4% paraformaldehyde (Alfa Aesar). The samples were sectioned to obtain 5 μm thickness, and immunolabeling was performed on serial sections to detect the presence of CCR7 (M1) and CD163 (M2) macrophage phenotypes in native tissues surrounding our implants using standard protocols provided by antibody manufacturers. The immunolabeled slides were examined and imaged using an inverted light microscope (Axio Vert.A1 Model, Zeiss). Fluorescence images were acquired for the test and control slides (data not shown) under the same exposure conditions. The images for the test samples were evaluated. Quantitative analysis was performed to obtain the number of cells expressing M1 only, M2 only, M1 and M2, or no M1/M2 phenotype. Here 4-5 areas per image (3 images were analyzed per test sample) of approximately 20-30 μm at the interface of the implants and native tissue (2-3 cell layers) were analyzed using a high-power microscope field (40x magnification). The total number of cells was determined by counting DAPI stained nuclei. The number of cells labeled positively for each marker(s) was also counted. The proportion of cells labeled with the specific marker(s) was determined as a percentage of the total number of cells in that region.

2.10. Long term stability testing of the hydrated crosslinked collagen microfibers

Crosslinked microfibers were de-spooled under tension onto cartridges. Six sterilized (see Section 2.7) cartridges were hydrated and mechanically tested (Section 4.3) to obtain mechanical properties of the microfibers before incubating the remainder of the sterilized cartridges in a petri dish containing Eagle's Minimum Essential Medium (EMEM) (ATCC, VA) supplemented with 1% Gibco™ Antibiotic-Antimycotic (ABAM) (Thermo Fisher Scientific) in

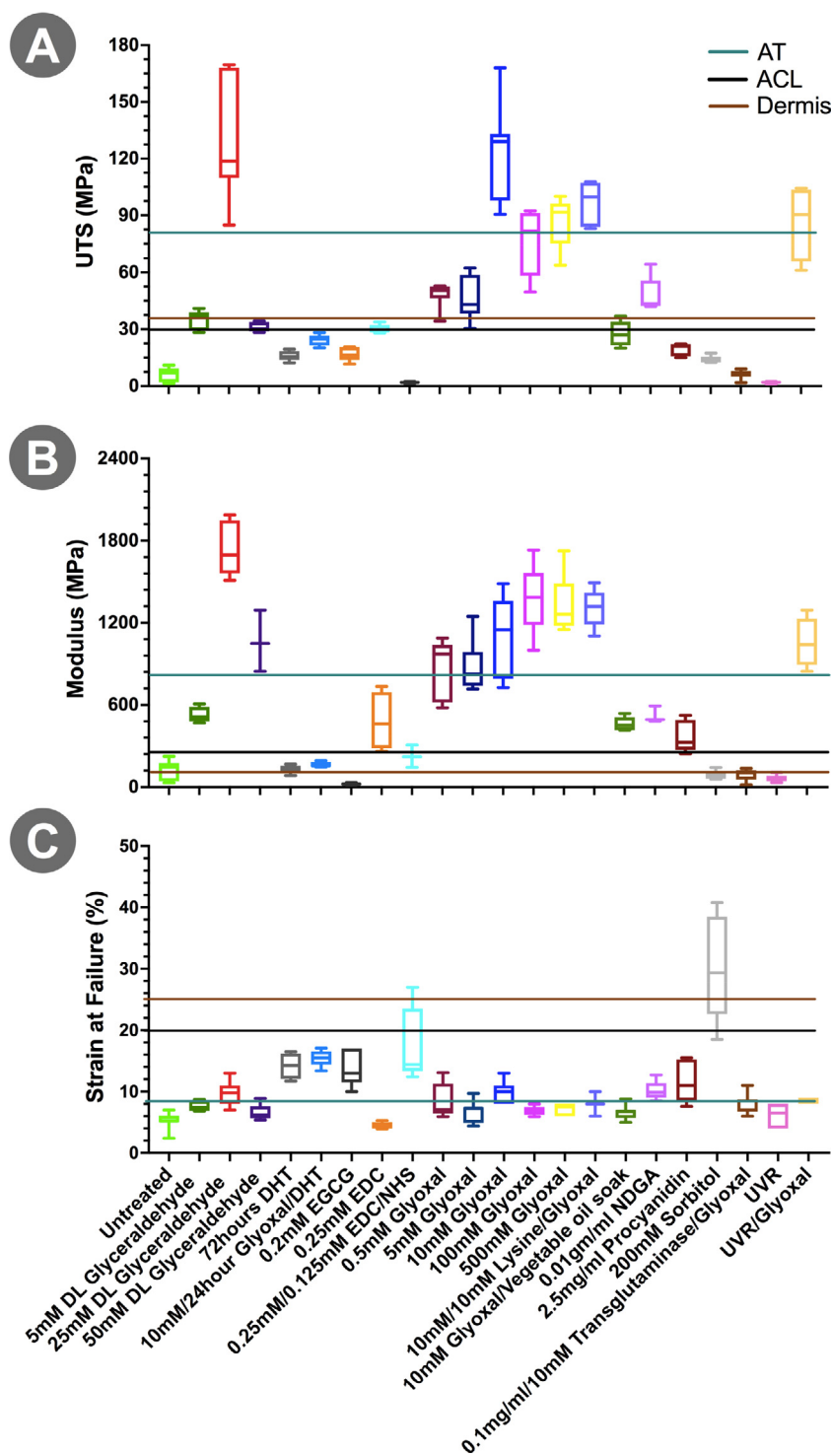


Fig. 1. Mechanical properties of representative crosslinked microfibers from 22 selected groups from Table 1. (A) UTS, (B) Modulus, and (C) % Strain at Failure of a single microfiber reveal strength tunable to meet or exceed human Anterior Cruciate Ligament (ACL) (black line), human Achilles Tendon (AT) (teal line) and human dermis (brown line) by changing crosslinking scenarios. Data represent four or more identical replicates, and error bars indicate S.E.M. (For interpretation of the references to color in this figure legend, the reader is referred to the web version of this article.)

an incubator maintained at 37°C and 5% CO₂. Throughout the experiment, cartridges were fully submerged and hydrated in sterile media. Six soaked cartridges were removed at 1 week, 1 month, 3 months, and 6 months to perform MTS testing. Simultaneously, microfiber diameters were measured (as described in Section 4.3) to determine the microfibers' swelling over time.

2.11. Statistical analyses

Two-way ANOVA followed by the posthoc Tukey's Multiple Comparison Test and unpaired two-tail t-test assessed tensile property differences for different crosslinker groups in Table 1 and Figs. 1 and 3. A priori, p values <0.05 were defined as significant.

All tests were performed using GraphPad Prism 7, and all parameters are expressed as Mean \pm Standard Error of the Mean (S.E.M.).

3. Results

3.1. Bio-manufacturing and mechanical properties

A microfluidic extrusion setup with coaxial flow consistently generated collagen microfibrils (Supplementary Fig. S1) for subsequent testing (Section 4.3). This approach yielded continuous microfibril production without defects for subsequent crosslinking.

To strengthen and stabilize the collagen microfibrils, we screened a wide range of conventional, new, and combination crosslinking conditions. Table 1 shows a summary of crosslinkers and the mean average hydrated Ultimate Tensile Strength (UTS) of 51 types of crosslinked microfibrils compared to the untreated/non-chemically crosslinked microfibrils using the testing method described in Section 4.3. Although the untreated group was not chemically crosslinked, air-drying the fibers after extrusion can result in covalent linking between triple helices (between alpha chains); a dehydrothermal crosslinking that occurs at room temperature. The data in Table 1 showed that different crosslinkers/crosslinking protocols (crosslinking *in situ* or post extrusion, range of crosslinker concentrations, and crosslinking time) affected the UTS of the microfibrils. The crosslinking condition with significantly high mean UTS amongst all the chemistries tested with that crosslinker is starred ($p < 0.01$) in Table 1.

Crosslinking procedures post extrusion with chemicals such as glyoxal (10mM and 72 hours post extrusion, 121.2 ± 7 MPa) and DL-Glyceraldehyde (25mM and 72 hours post extrusion, 128 ± 12 MPa) resulted in microfibrils with UTS nearly 20-fold higher than the untreated/non-chemically crosslinked microfibril (6.1 ± 1 MPa). Notably, crosslinking using EDC and EDC/NHS on microfluidic microfibrils using our extrusion setup yielded UTS values of 16.6 ± 2 MPa and 30.2 ± 1 MPa, respectively, which are significantly lower than the glyoxal and DL-Glyceraldehyde. *In situ* (crosslinked mixed with collagen during wet extrusion) crosslinking using chemical crosslinkers such as choline bitartrate (1mM or 100mM), EGCG (200 μ M or 1mM), and D-sorbitol (200mM) resulted in a significant decrease ($p < 0.01$) in UTS compared to untreated microfibril. Physical crosslinking techniques such as dehydrothermal treatment (DHT) (3 days, 16.2 ± 1 MPa) post extrusion also yielded microfibrils stronger than the untreated microfibril. Still, they were weaker than the chemical crosslinking groups using glyoxal and DL-Glyceraldehyde described above. Ultraviolet Radiation (UVR) treatment (1.9 ± 0.2 MPa) of methacrylated collagen microfibrils post extrusion also yielded fibers significantly weaker than untreated telocollagen microfibrils ($p < 0.01$).

With glyoxal crosslinking producing the highest UTS, we further tested glyoxal crosslinking *in situ* (alone or with L-Lysine or D-Sorbitol) and physically crosslinked fibers (DHT and UVR) with 10mM glyoxal for various time points to explore any effects on strength change. Adding crosslinking with glyoxal to these methods increased the UTS of all these groups, with the most significant increase ($p < 0.01$) observed for L-Lysine (10mM, 2 hours)/Glyoxal (10mM, 24 hours) (96.9 ± 5 MPa) and UVR (0.3 hours)/glyoxal (10mM, 24 hours) (86.6 ± 10 MPa) groups. However, none of these groups were as strong as crosslinking with glyoxal alone.

We compared mechanical properties (Fig. 1) from crosslinker groups tested in Table 1 to values reported for human ACL [54,55], Achilles tendon [56], and dermis [57]. Results revealed that the average (mean) wet UTS of collagen microfibrils for select crosslinking groups, notably, 10 mM glyoxal with or without 10mM L-Lysine *in situ*, and 25mM DL-Glyceraldehyde are equal to or greater than reported UTS of human ACL, AT, and dermis.

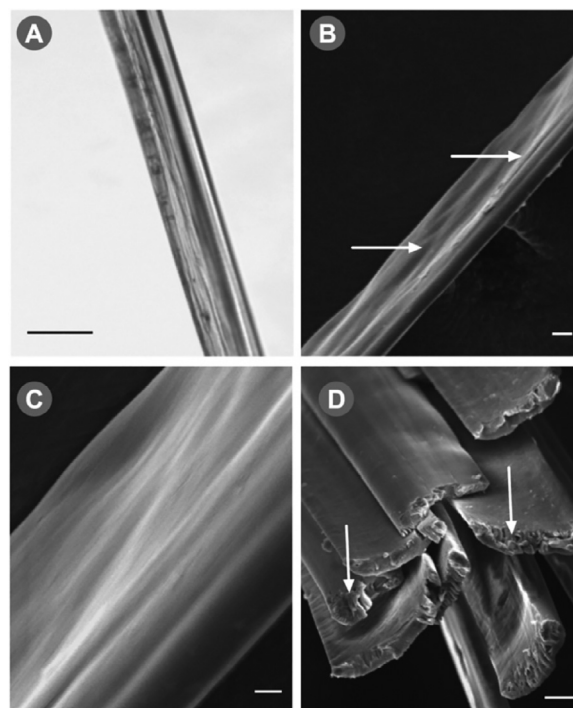


Fig. 2. Telo GLY microfibril(s) depicting ultrastructural features. Light microscopy image of a single dry extruded crosslinked microfibril (A), SEM images of a dry microfibril (B) and (C), a cross-section of bundled microfibrils soaked for 30 minutes in DPBS (D) reveals structural details with consistent, uniform, and ribbon-like microfibrils produced. Arrows indicate microfibril crevice and ridges. Scale bars are (A) 50 μ m, (B) 10 μ m, (C) 3 μ m and (D) 20 μ m.

Four crosslinking conditions selected from the initial screen (Table 1 bolded and Fig. 1) were chosen for further investigation, chosen for overall optimal biomechanical performance, processing time, complexity, and cost. The selected crosslinking groups are (1) telocollagen crosslinked with 10mM glyoxal for 72 hours (**Telo GLY**), (2) telocollagen crosslinked with 25mM DL-Glyceraldehyde for 24 hours (**Telo DLG**), (3) atelocollagen crosslinked with 10mM glyoxal for 24 hours (**Atelo GLY**), (4) atelocollagen crosslinked with 25mM DL-Glyceraldehyde for 72 hours (**Atelo DLG**) and (5) telocollagen crosslinked with 0.25mM EDC for 24 hours (Telo EDC) and compared to untreated microfibrils and dry Telo GLY fibers. EDC is included for comparison as it is commonly used in the collagen TEMP field [42,49,58].

3.2. Characterization of microfibril ultra-structure using a light microscope and SEM imaging

With basic crosslinking formulations optimized for future analysis, a high draw collection apparatus to draw the collagen fibers onto a flat solid spool (Supplementary Fig. S2) was used to maximize subsequent studies' fiber material properties. Collecting crosslinked fibers on the grooved drum produced thin, ribbon-like microfibrils (Fig. 2). Light microscopy imaging (Fig. 2A) and SEM imaging (Fig. 2B) confirmed the dry microfibril's homogeneous width along the longitudinal axis. Fig. 2B and high magnification SEM (Fig. 2C) imaging of longitudinal section revealed parallel alignment of ridges and crevices within the dry microfibril. Fig. 2D highlights cross-sectional features of hydrated extruded crosslinked microfibril bundle using SEM. These images showed ultrastructural features of an external smooth surface with apparent fibrous sub-fiber structure, demonstrating that extruded crosslinked microfibrils are consistent, thin, and ribbon-like.

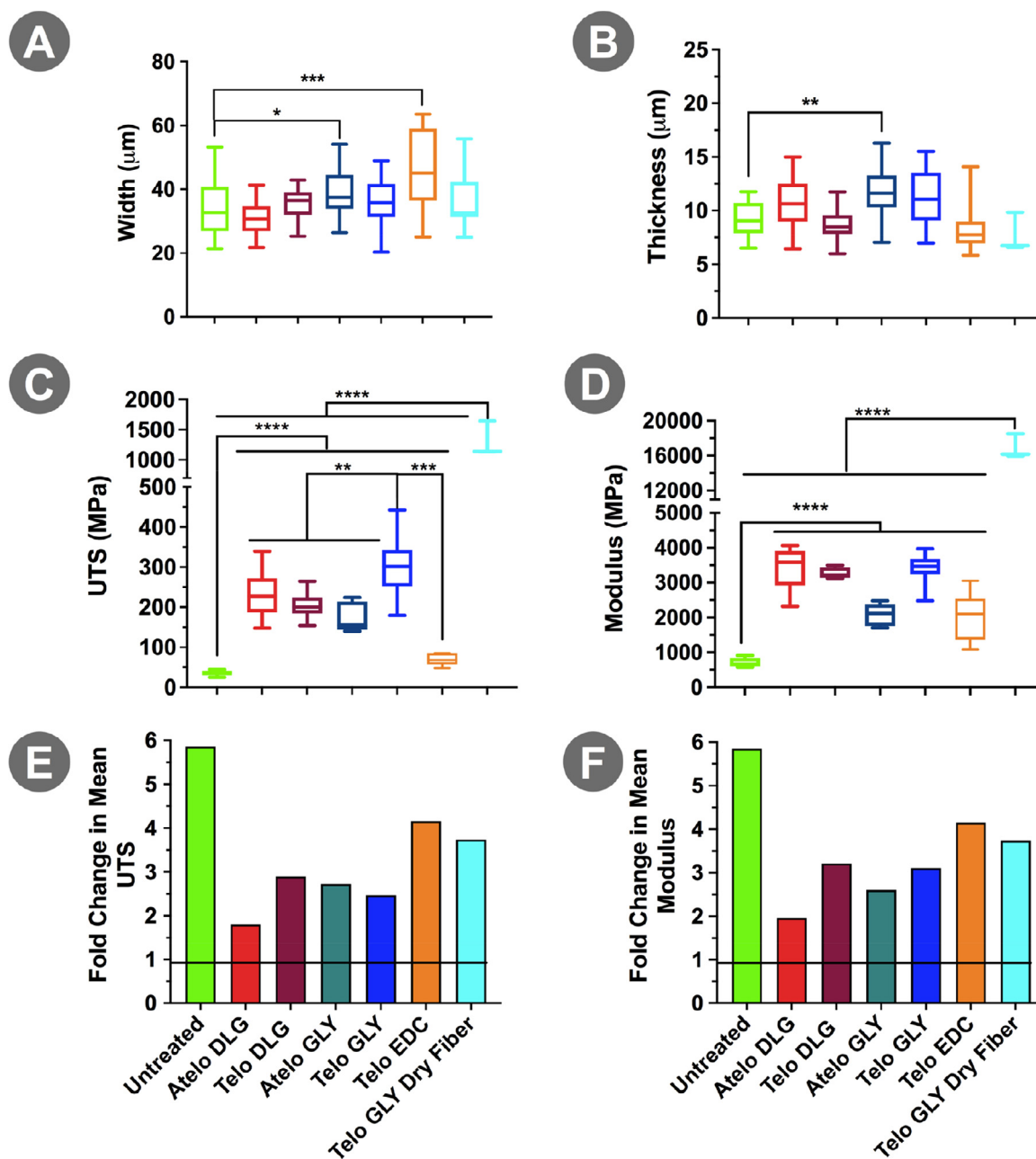


Fig. 3. Changes in ribbon-like collagen fibers' mechanical properties from select crosslinking groups (see text) post-optimization of microfiber collection onto a flat solid spool. There was a significant increase in the tensile properties of all the extruded microfibers. The untreated microfiber group demonstrated the greatest change in mean UTS and modulus compared to other crosslinker groups. Values of width (A) and (B) thickness of the microfibers were used to evaluate (C) UTS and (D) Modulus of crosslinked microfibers soaked for 30 minutes in DPBS. (E) and (F) demonstrate a significant change in mechanical properties compared to the data reported in Fig. 1. Results are shown as Mean ± S.E.M. and are representative of 3 replicates from 2 or more separate experiments. (*p<0.05, **p<0.01, ***p<0.005 and ****p<0.0001).

Optimization of crosslinking chemistry and collection methods ultimately led to significant differences in mechanical properties (Fig. 3). The width and thickness of hydrated microfibers (Fig. 3A and B) measured from representative images such as those shown in Fig. 2A-C were used to calculate the improved UTS and modulus (Fig. 3C and D). When compared to the wet untreated (34.1 ± 2 µm) microfibers, wet Atelo GLY (39.2 ± 1 µm) and Telo EDC (46.4 ± 2 µm) microfibers showed a significantly higher width (p<0.05). Wet Atelo GLY microfibers were also significantly thicker (11.9 ± 0.5 µm) than the untreated microfibers (9.2 ± 0.5 µm) (p<0.01). Fiber thickness of Telo GLY (11.1 ± 0.5 µm), Telo DLG (8.6 ± 0.2 µm) and Atelo DLG (10.9 ± 0.4 µm), as well as widths of Telo GLY

(36.1 ± 0.7 µm), Telo DLG (35.4 ± 0.8 µm) and Atelo DLG (31.1 ± 1 µm) hydrated microfibers were similar to that for the untreated fiber. The most significant change in UTS was observed for untreated fibers; mean UTS and modulus increased from 6.1 ± 1 MPa and 119.8 ± 23 MPa to 35.8 ± 3 MPa and 701 ± 53 MPa. Microfibers from groups such as Telo GLY (121 ± 7 MPa UTS and 1103 ± 63 MPa modulus to 299 ± 15 MPa and 3431 ± 86 MPa respectively) and Atelo DLG (128 MPa UTS and 1734 ± 79 MPa modulus to 231 ± 18 MPa and 3408 ± 185 MPa respectively) demonstrated at least a 2-fold increase in mean UTS and modulus (Fig. 3E and F). There was no change in the strain at failure (%) for all groups tested.

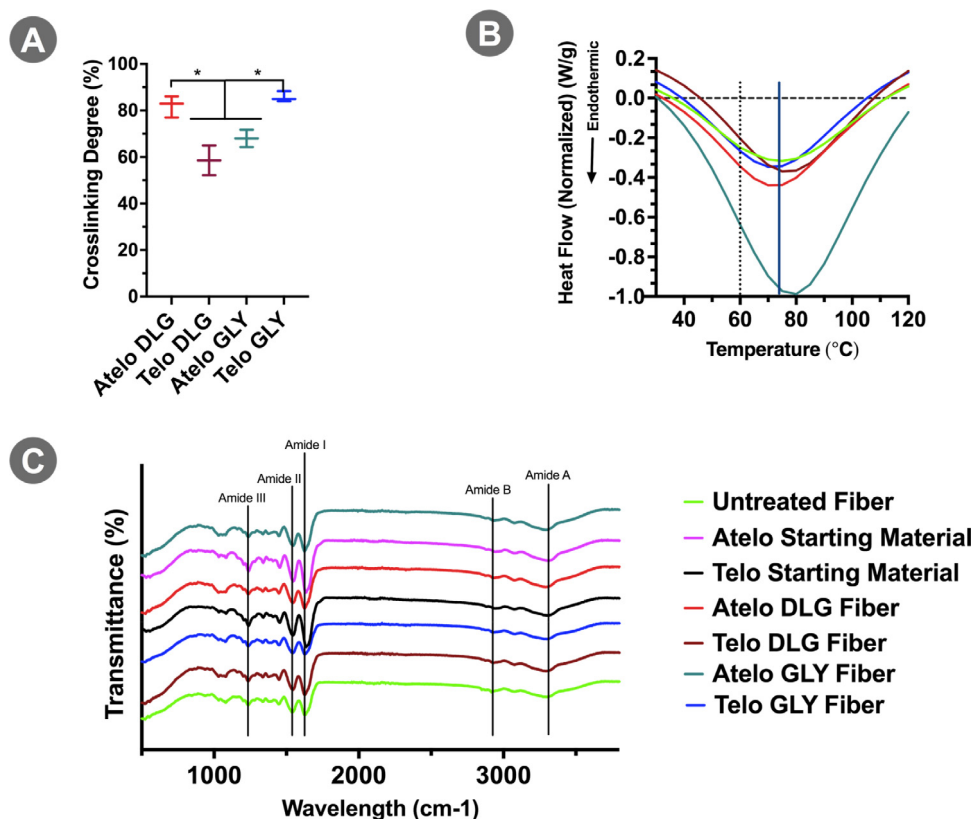


Fig. 4. Degree of crosslinking and biophysical characterization of crosslinked microfiber groups. (A) The crosslinking degree of extruded microfibers was compared to the untreated microfiber (0%) using the ninhydrin assay determines free amino groups in the microfiber. Telo GLY and Atelo DLG groups demonstrated maximum crosslinking degrees compared to Telo DLG and Atelo GLY. (B) Thermal denaturation scans of extruded microfibers compared to the untreated microfibers show a small increase in melting temperatures. The melting temperature of human AT (solid vertical line) is significantly lower than the extruded microfibers' average melting temperature (dotted line). ATR-FTIR spectra (C) of untreated and crosslinked microfibers compared to Type I collagen starting material (freeze-dried, unprocessed). Data in (A) is shown as Mean \pm S.E.M. and represents three replicates from two separate experiments. (* $p < 0.05$).

3.3. Degree of crosslinking, biochemical and biophysical characterization of the crosslinked microfibers

A ninhydrin assay was used to assess the crosslinking degree (Fig. 4A) biochemically. Telo GLY ($86 \pm 1\%$) and Atelo DLG ($82 \pm 3\%$) microfibers demonstrated a significantly higher degree of crosslinking compared to Atelo GLY ($68 \pm 4\%$) and Telo DLG ($59 \pm 6\%$), highlighting that higher time of crosslinking improved crosslinking efficiency. SDS-PAGE subsequently assessed the primary and secondary protein structure of the extruded collagen microfibers. Analysis of the acidified starting material confirmed primary collagen alpha, beta, and gamma chains present in the crosslinked collagen fibers (Supplementary Fig. S4A). However, due to the microfibers' inability to be dissolved in 0.05M acetic acid, collagen was not present in the microfiber acid extracts. To further explore this, we attempted to dissolve the microfibers (untreated and crosslinked) in a variety of solvents at room temperature (RT) as well as 37°C for 24–48 hours with stirring. We tested 10mM HCl, 100mM HCl, 0.5M Acetic acid and 1M Acetic Acid. While the untreated fibers readily dissolved in 100mM HCl, 0.5M Acetic acid, and 1M Acetic Acid both at RT and 37°C within 24 hours, the crosslinked fibers dissolved minimally (<2%) only at 37°C after 48 hours. SDS-PAGE analysis (Supplementary Fig. S4B) confirmed the presence of α , β , and γ regions for the untreated hydrolyzed material and very faint bands of α regions compared to the starting material.

Since our crosslinked collagen microfibers were resistant to acid hydrolysis, we performed limited pepsin digestion and collagenase

digestion to explore if our extruded microfibers retained partial or complete triple-helical structure characteristic of type I collagen in connective tissues [19,59–61]. Supplementary Fig. S5 demonstrates that the un-crosslinked and the Telo GLY fibers were completely digested using collagenase *in vitro*. Supplementary Fig. S6 demonstrates that the untreated Telo fibers were partially digested with pepsin at 2 hours with visible alpha bands on SDS-PAGE. However, the Telo GLY fibers were not digested in the presence of pepsin, as seen by the lack of bands on the SDS-PAGE gel in Supplementary Fig. S6. These results suggest that our extruded microfibers retained a significant part of the native triple-helical structure post glyoxal crosslinking.

Biophysical characterization using differential scanning calorimetry (DSC) measurements on extruded microfibers revealed an insignificant increase in melting temperatures between the untreated and the crosslinked microfiber groups (Fig. 4B). However, the average melting temperature of all the extruded microfibers ($74 \pm 3^\circ\text{C}$) was significantly higher than that for the human AT (60°C) [62], indicating improved overall structural stability [63]. ATR-FTIR spectral analysis (Fig. 4C) showed amide I peak at $\sim 1628\text{ cm}^{-1}$, amide II peak at $\sim 1542\text{ cm}^{-1}$, amide III peak at ~ 1237 , amide A peak at $\sim 2944\text{ cm}^{-1}$, and amide B peak at $\sim 3298\text{ cm}^{-1}$ for the untreated and the crosslinked microfibers. These values were not significantly different from the starting material, indicating that microfibers' secondary structure was unchanged after the extrusion and the crosslinking process used in this study.

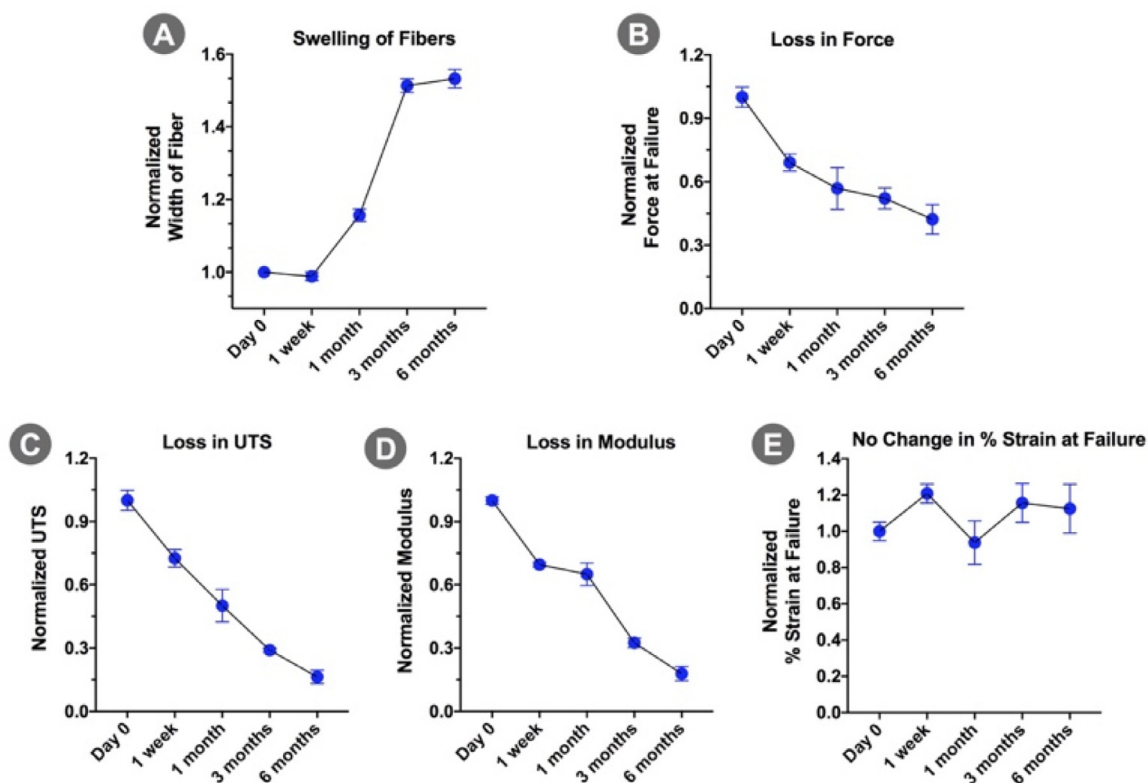


Fig. 5. Mechanical stability of Telo GLY microfibers incubated in sterile EMEM and under tension assessed after 1 week, 1 month, 3 months, and six months in a humidified incubator at 37°C and 5% CO₂ show that Telo GLY microfibers at the end of 6 months swell by 50% (A), lost 60% of the Force at Failure (B), 80% of UTS (C) and 80% of Modulus (D) compared to Day 0. However, there was no significant change in % Strain at failure at the end of 6 months. All the values depicted in A-E have been normalized to a value of 1 for Day 0. The continuous lines in A-E are drawn by inspection only to serve as a guide to the reader. Data are shown as mean ± S.E.M. and are representative of at least five replicates.

3.4. Effect of long-term hydration of microfibers in culture media on mechanical properties and degree of swelling

With Telo GLY microfibers showing optimal mechanical properties, this group was further tested for long-term stability mimicking *in vitro* physiological conditions. There was no significant difference in the Telo GLY fibers' mechanical properties before and after E-beam sterilization (see Section 2.10). Incubation in EMEM for six months at 37°C led to an increase (swelling) in microfiber width by 53% ($36.4 \pm 1.1\mu\text{m}$ on Day 0 to $56.0 \pm 1.6\mu\text{m}$ at six months) as shown in Fig. 5A. The swelling was accompanied by an expected decrease in mechanical properties due to the increase in cross-sectional area. However, the mean force at failure decreased by only 54% from its initial value in 6 months (Fig. 5B). Mean UTS and modulus were reduced by 82% from the starting point in 6 months (Fig. 5C and D). There was no significant change in the strain at break (%) between Day 0 and 6 months of incubation (Fig. 5E). Fig. 5 further shows that Telo GLY microfibers have not wholly dissolved when incubated in an *in vitro* simulated biological environment for up to 6 months.

3.5. Tenocyte survival and cytotoxicity of the extruded microfibers

Human tenocytes were used to assess collagen fiber cytocompatibility, which was highly compatible via multiple assays. No significant change in tenocytes' survival over 7 days was noted by AlamarBlue fluorescence (Fig. 6A) compared to the positive control (Cells only group). However, survival for cells growing with microfibers from selected fiber groups was significantly higher ($p < 0.05$) than that for negative controls (10mM glyoxal chemical [neat] and ZDBC film). Tenocytes viability was between 75% and

85% on glyoxal crosslinked collagen fibers compared to tenocytes growing on culture plastic (100%) when assayed using the MTT reagent (Fig. 6B). The negative controls (10mM GLY chemical and ZDBC film) demonstrated significantly lower ($p < 0.005$) tenocyte survival than the "Cells Only," Telo DLG, Atelo GLY, and Telo GLY groups. Similar results were observed using LDH assay (Fig. 7C) wherein all the extruded microfiber groups except for Atelo DLG and Telo DLG elicited tenocyte viability similar to the "Cells Only" group. At the end of 7 days, the 10mM GLY chemical group did not have enough tenocytes (ND) to be assayed by LDH release into the media. We also used a commercially available coated Vicryl suture from Ethicon, typically recommended in wound closure, for comparison. Results indicated that our microfibers exhibited significantly lower cytotoxicity ($p < 0.005$) than the suture using both LDH and MTT assays (Fig. 6B and C). Overall, our study used multiple assays to establish cytocompatibility of the extruded microfibers. The attachment of tenocytes on Telo GLY microfibers with elongated morphology is shown in Fig. 6D-E, indicating that the fibers imparted alignment along the fibers.

3.6. Subcutaneous implant biocompatibility and macrophage polarization

All implants appeared macroscopically normal at collection, with no notable macroscopic defects at the implant site or nearby lymph nodes. Microscopic lesions were also absent in the lymph nodes. All implants were microscopically scored using H&E staining as having not appreciably degraded. Encapsulation was absent in collagen fiber groups (Severity Score average of 1), although encapsulation was moderate to marked in FiberWire™ implants (Severity Score average of 3.5).

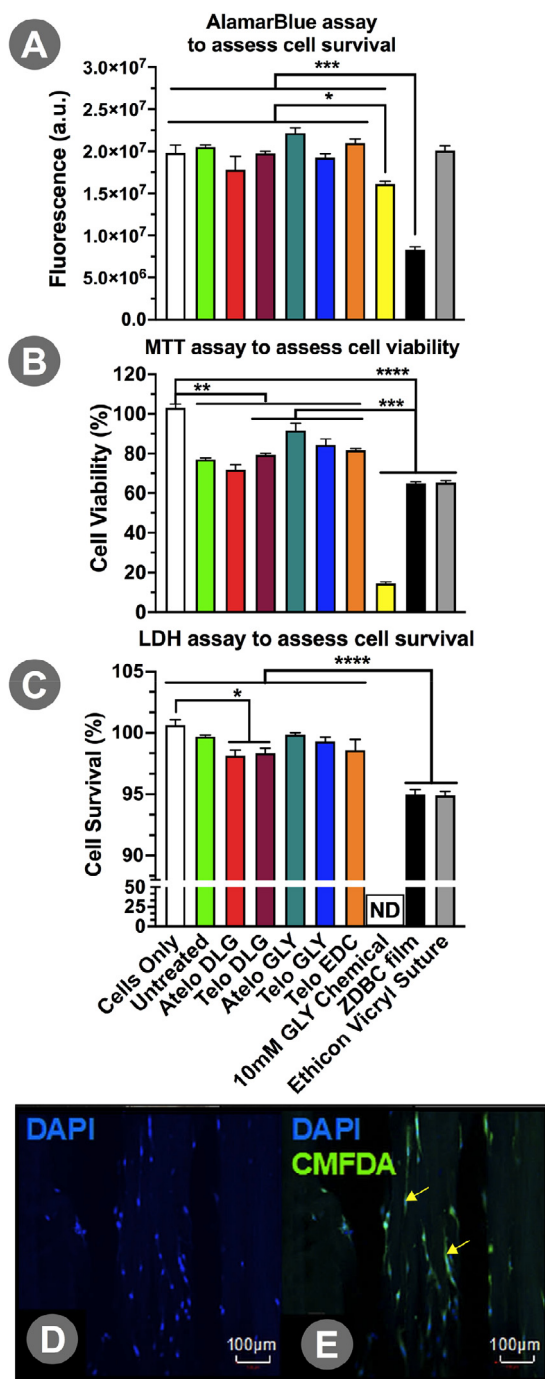


Fig. 6. Effects of crosslinked microfibers on viability, toxicity, and tenocyte attachment. (A) shows no significant change in survival of human tenocytes incubated with the crosslinked microfibers assayed using AlamarBlue after 7 days of incubation compared to the cells-only group. Survival was significantly lower in tenocytes incubated with negative controls (ZDBC film and 10mM GLY chemical) and vicryl suture than the microfiber groups. MTT assay results (B) also revealed a decrease in viability for tenocytes incubated with the microfiber groups compared to the cells-only group but a significant increase compared to negative controls. On the other hand, LDH assay results (C) show a significant decrease in cell survival for the Atelo DLG, Telo DLG microfiber groups, and the negative controls. Both MTT and LDH assays were performed at 7 days post-incubation with tenocytes. All data in (B) and (C) was normalized to the cells-only group. (ND) indicates that the 10mM Glyoxal chemical treatment group had a significant arrest in proliferation resulting in an insufficient number of cells to detect LDH at the end of the assay timepoint. (* $p < 0.05$, ** $p < 0.01$, *** $p < 0.005$ and **** $p < 0.0001$). (D) and (E) show representative confocal images of human tenocytes attached to Telo GLY microfibers, with DAPI and live-cell stain, respectively, showing cytoplasmic extensions and elongated nuclei.

Scoring inflammatory cells and markers (0 = absent to 4 = severe) in the collagen fiber implant sites showed little inflammation in or around the implants, with a macrophage response proximal to the implanted fibers. Collagen fibers were infiltrated with dense collagen that was well-integrated with the host tissue, along with some neovascularization. FiberWire™ suture implant sites there were marked by a foreign body giant cell response, vascularity, loose connective tissue and accompanying fat formation around the sutures.

Overall, microscopically, the FiberWire™ suture test article caused a pronounced, near three-times higher reaction (reactivity score of 19) in the tissue as compared to the mild reaction for collagen suture crosslinked by glyoxal (reactivity score of 7), and over twice the inflammatory reaction or DL-glyceraldehyde crosslinked collagen fibers (reactivity score of 10) per **Table 2**.

Immunostaining was used to determine macrophage polarization extents in native tissue around microfiber implants from 4 crosslinker groups. **Fig. 7A and B** are representative immunofluorescent images showing expression patterns of CCR7 (M1) and CD163 (M2) macrophage phenotype in the native tissue of rats surrounding Telo GLY microfiber implants at four weeks, while **Fig. 7C and D** show the same for Atelo DLG microfiber implants. **Fig. 7E** shows quantitation of the percentage of macrophages that expressed M1 and M2, M1 only, M2 only, or no M1/M2 phenotype. Glyoxal crosslinked groups (Telo GLY and Atelo GLY) demonstrated a significantly higher proportion of macrophages expressing M1 and M2 phenotype (~40%) compared to the DL-Glyceraldehyde crosslinked groups (Telo DLG and Atelo DLG) (**Fig. 7C**). Furthermore, between the Telo GLY and Atelo GLY group, Telo GLY implants elicited a small subset of cells expressing M2 only phenotype (6%), while the rest of the groups had negligible M2 only phenotype; Atelo GLY (0.2%), Telo DLG (0%) and Atelo DLG (0%) (**Fig. 7E**). There was a significantly higher proportion of cells with M1 phenotype in the DL-Glyceraldehyde crosslinked groups; Telo DLG (64%) and Atelo DLG (58%) compared to the glyoxal crosslinked groups; Telo GLY (24%) and Atelo GLY (19%). Staining with appropriate controls revealed negligible non-specific background staining (not shown). Sectioning artifacts of the suture control samples and significant background staining made it challenging to perform this analysis.

3.7. Development of higher-order structures with collagen microfibers

With the collagen yarn feedstock manufacturing and glyoxal crosslinking optimized at this stage, the ability to form secondary or tertiary structures with these collagen filaments using textile braiding equipment was explored. Fifty-six collagen fiber strands were successfully able to be braided into a 435 μ m suture (at a gauge size of a 4-0 suture per USP<861>), either as a pure collagen suture or as mixed with polymer strands (**Fig. 8A and B**). **Fig. 8C and D** show SEM images of the braid at various resolutions, showing high fiber organization and an absence of fiber damage from braiding. **Fig. 8E** shows an SEM image of a knot with the braided collagen suture. **Fig. 8F** shows the stress-strain curve after mechanically testing the braided suture. The suture exhibits a high retained strength post-braiding at over 80 MPa of stress at break configured as a pure collagen fiber braid with the initial braiding pattern and loading configuration.

4. Discussion

We report developing a high output microfluidic extrusion process to manufacture strong, biocompatible type I collagen microfibers suitable for surgical suture and possibly other biotextile manufacturing. This extensive crosslinking study reveals that the bio-manufactured glyoxal crosslinked telocollagen microfibers

Table 2
In Vivo Biocompatibility determined using ISO 10993-6 scoring on H and E stained slides at four weeks post-implantation.

ISO 10993-6 Scoring	FiberWire™ Suture	Telo GLY Fibers	Atelo DLG Fibers
INFLAMMATION Polymorphonuclear	1	0	0
Lymphocytes	0	0	0
Plasma Cells	1	0	0
Macrophages	2	2	2
Giant Cells	2	0	1
Necrosis	1	0	0
SUBTOTAL (X2)	14	4	6
Neovascularization	2	2	2
Fibrosis	1	1	1
Fibrotic Encapsulation	2	0	1
Fatty Infiltrate	0	0	0
SUBTOTAL	5	3	4
TOTAL	19	7	10

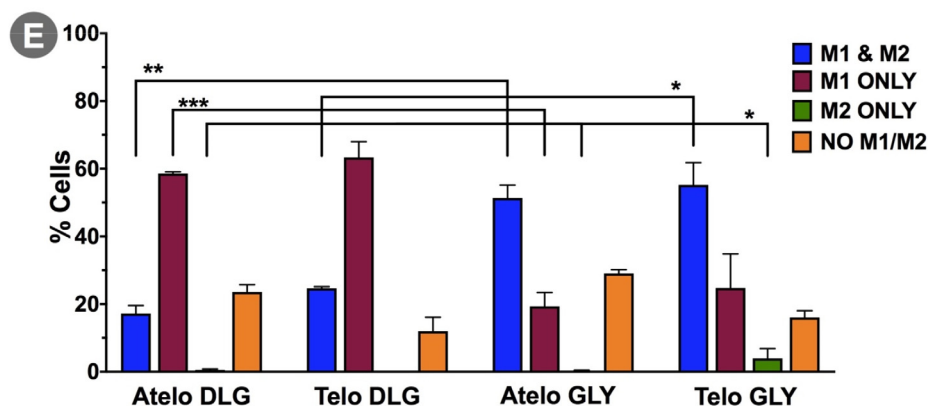
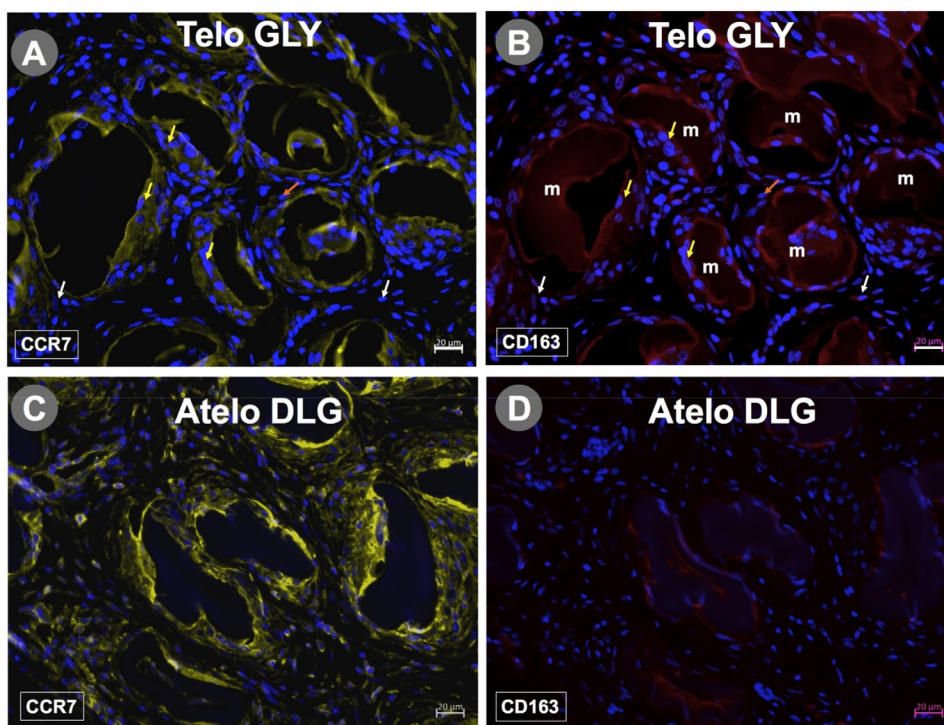


Fig. 7. Representative immunofluorescent images showing examples of the host macrophage response to the Telo GLY microfibers (m) (A and B) and Atelo DLG (C and D) at four weeks. Arrows indicate examples of cells expressing both M1 and M2 (yellow), M1 only (orange) and M2 only phenotype (white) (Scale bar = 20 μm) CCR7 (M1) = yellow, CD163 (M2) = red, DAPI (nuclei) = blue. m denotes microfiber bundles. (E) shows the % of cells expressing M1 and M2, M1 only, M2 only, or no M1/M2 phenotype for the four groups of crosslinked microfibers. Results from this analysis show initiation of pro-regenerative M2 macrophage phenotype in all microfiber groups tested. Glyoxal crosslinked fiber groups showed a higher proportion of M1 and M2 phenotype cells than the DL-Glyceraldehyde crosslinked fiber groups. Furthermore, the Telo GLY group had a small but significant subset of M2-only macrophages. Expression of CCR7 was used as a marker for M1 and CD163 as a marker for M2. (*p<0.05, **p<0.01, and ***p<0.005). (For interpretation of the references to color in this figure legend, the reader is referred to the web version of this article.)

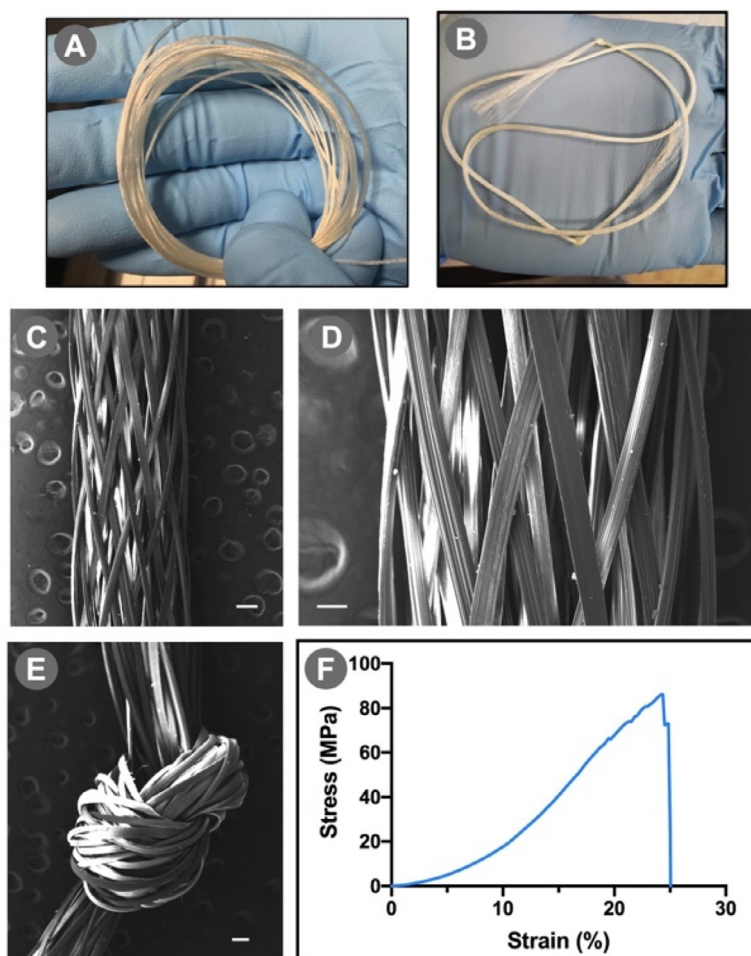


Fig. 8. Braided Collagen Fibers. (A) and (B) show pictures of size 4-0 braided suture using 56 collagen fiber strands. (C) and (D) show representative SEM images of the braided suture at two different magnifications. SEM image shows a tight knot tied in the collagen suture (C). Panel (D) shows the stress vs. strain (%) curve for the braid. Scale bars: (C) 200 μ m, (D) 100 μ m and (E) 200 μ m.

Table 3

Mechanical tensile properties (hydrated) of strongest collagen fibers made with different crosslinkers in the literature compared to the present study.

Reference	Crosslinker/Crosslinking Method	UTS (MPa)	Modulus (MPa)	Strain at Failure (%)
Present Study	Glyoxal	299 \pm 15	3431 \pm 86	9.5 \pm 1.6
Yaari et al. [66]	Glutaraldehyde	151 \pm 31	888 \pm 153	20.5 \pm 2
Ahmad et al. [49]	EDC ^a	150 \pm 100	1000 \pm 600	18 \pm 12
Wang et al. [64]	DHT	92 \pm 31	895 \pm 206	12 \pm 2
Koob et al. [53]	NDGA	91 \pm 10	696 \pm 38	11 \pm 1

^a Values were estimated from graphical data published. Exact values were unavailable.

demonstrate dry and wet-tensile properties superior to prior crosslinked collagen extruded microfibers [38,39,42–44,49,64–66] (Table 3). While some previous studies obscured whether tensile testing was performed on hydrated or dry fibers or how the fibers were wetted if fully hydrated, we show both the dry and hydrated properties of our optimized crosslinked fibers with a detailed testing methodology.

As crosslinking has been shown to change the mechanical strength of collagen-based biomaterials [40], we tested a plethora of common and uncommon crosslinkers and crosslinking conditions (Table 1) encompassing chemical (glyoxal, DL-Glyceraldehyde), physical (UVR, DHT), and enzymatic (transglutaminase) techniques. Fig. 1 shows that the UTS and modulus of collagen microfibers made using our high output microfluidic extrusion

setup can be varied over 200-fold by selecting a specific crosslinking condition.

The changes made to scale-up manufacturing on a grooved solid drum led to significant alterations in all the crosslinked microfibers' structural and hydrated mechanical properties (Figs. 2 and 3). Mechanically, this improved strength may be related to tempering, thinning, and improved molecular alignment to ribbons, which were once cylindrical, resulting in fiber tensile properties stronger than the human ACL, Achilles tendon, dermis, or any other soft connective tissue. Microfibers surface morphology has previously been shown to be dependent on crosslinking techniques used [39]. Chemical crosslinking of collagen microfibers results in dry microfibers with prominent ridges and crevices along the microfibers' longitudinal axis, such as that seen in our case. This type

of structural morphology has been shown to facilitate cell attachment and fibroblast migration [58,67].

While prior studies focus predominantly on crosslinking strategies to enhance extruded fibers' mechanical properties [22,42,49], emphasis on determining the degree of crosslinking mechanism efficiency is lacking. Insufficient crosslinking can lead to lower tensile strengths, while chemical crosslinker overuse can lead to crosslinker residues on the microfibers' surface, resulting in cytotoxicity. Here, we performed the ninhydrin assay (Fig. 4A) and observed that groups with maximum crosslinking degrees were those that were crosslinked for 72 hours (Telo GLY and Atelo DLG), which also correlated with a significant increase in tensile strength. The chemistry of crosslinking using aldehydes involves forming Schiff's base type compounds with functional amino groups in collagen, leading to strong molecular bonds [68]. Chemical analysis of our extruded microfibers revealed that only the crosslinked microfibers (unlike the starting material or the untreated microfibers) were resistant to acid hydrolysis. Thus, our microfluidics setup generated microfibers with chemical stability higher than the lyophilized starting material suggesting tight packing of the collagen molecules in the microfibers resulting in a stable higher-order structure with possibly low internal moisture content.

The neutralizing formation buffer used in this study contains 10% PEG (Section 4.1). Molecular crowding, achieved by the addition of PEG, during self-assembly of collagen monomers may result in more efficient packing and alignment of the fibers [69]. Such higher-order structure has been reported in native connective tissues [2,70]. Limited peptic digestion of the collagen microfibers suggests native triple-helical structure preservation post extrusion and crosslinking. ATR-FTIR spectral peaks of the starting lyophilized material and the extruded fibers presented in Fig. 4C also indicated that neither the extrusion process nor the crosslinking technique changed collagen structure significantly relative to the native collagen starting material, showing native-like collagen fibril formation.

We show proof-of-concept that our optimized collagen microfibers, crosslinked with the glyoxal crosslinker by a Maillard reaction [71], can be used in textile-style manufacturing to form a braid (Fig. 6). While glyoxal has previously been used to crosslink collagen/chitosan composite hydrogels for bone tissue engineering [52], this is the first report to demonstrate glyoxal use to bioengineer additively manufactured collagen microfiber intended for biotextiles (e.g. bioactive suture or sheets). We produced a continuous 10 kilometers of clinical grade collagen as fibers without breaks, showing promise for large-scale manufacturing of a first-ever collagen microfiber-based braided suture made with biocompatible glyoxal crosslinking. The resulting braid was pliable, strong, and easily tied with a simple surgeon's knot and could be used with bone anchors to internally brace a ligament. The collagen braid UTS exceeds that of native ligament and tendon tissues. The collagen suture exhibited an increased strain at break relative to the individual feedstock fibers, as expected by the pure collagen braided suture's imparted loose braiding structure in these prototypes.

Augmenting suture repair of ligaments or tendons with collagen-based microfibers or using a collagen-based braided suture in wound healing requires them to support the tissue mechanically and promote tissue remodeling at a reasonable rate [38]. *In vitro* and *in vivo* biocompatibility tests are critical to establishing these chemically crosslinked microfibers' effects on cytotoxicity, inflammatory and healing response. Multiple assays indicated that our extruded microfiber bundles were cytocompatible, with minimal toxicity to human tenocytes. Microfluidic extruded microfibers further supported human tenocytes' attachment and assumed the elongated shape observed on connective tissue [20].

Biocompatibility is defined as the ability of an implant to "locally trigger and guide non-fibrotic wound-healing, reconstruction,

and tissue integration" [72]. Microfiber biocompatibility was examined following subcutaneous implantation in rats at four weeks. Per ISO 10993 scoring, crosslinked microfiber bundle implants exhibited very low (glyoxal groups) to low (DL-glyceraldehyde groups) inflammatory response. The glyoxal-telocollagen fiber group (Telo GLY) demonstrated a pro-regenerative response. Additionally, long-term stability data and rat histology images indicated microfiber stability for up to at least 6 months *in vitro* and 4 weeks *in vivo*. Another important metric for new biomaterial characterization is evaluating its hemolytic properties to ensure that it does not cause erythrocyte hemolysis. This will be addressed in subsequent studies from our group.

Macrophages are a heterogeneous mix of mononuclear cells activated in the host due to tissue damage [73,74] such as, during implantation of materials. Previous studies have highlighted the importance of determining macrophage phenotype polarization at the implant and host tissue interface [75,76] to assess the host's potential to overcome pro-inflammatory signals and transition towards tissue repair remodeling in response to the surgical implant. Macrophage phenotype has been broadly characterized as pro-inflammatory M1 macrophages and regenerative M2 macrophages with immunoregulatory or tissue remodeling characteristics [77]. However, it is essential to note that activated macrophages have the plasticity to switch from M1 to M2 and M2 to M1 phenotypes easily triggered by changes in the local microenvironment [78,79]. Due to this, macrophages may also adopt transitional characteristics of both M1 and M2 phenotype [80]. We determined the proportion of cells exhibiting M1, M1, and M2 or M2 phenotypes in the current study. We thus inferred that at 4 weeks of implantation, the glyoxal crosslinking groups had cells with more M1 and M2 or M2 only phenotype indicating that the host had initiated a tissue remodeling response at 4 weeks. Therefore, we conclude that the microfibers from the glyoxal groups were the most biocompatible. To the best of our knowledge, such in-depth analysis of immunologic response has not been performed using crosslinked collagen microfibers.

5. Conclusion and clinical significance

In this study, using clinical-grade commercially available type I collagen, we report an advanced microfluidic extrusion process for bio-fabricating type I collagen microfibers. Glyoxal crosslinked collagen fibers exhibit superior tensile properties, biocompatibility and manufacturability. Glyoxal, a metabolic byproduct of glycolysis, is well known to interact with collagen, particularly in connective tissues. However, this is the first report demonstrating this native tissue crosslinker's extraordinary ability to produce strong, cytocompatible, and biocompatible collagen microfibers from microfluidic wet-extrusion that are ideally suited for clinical use as a biotextile or suture. This high output collagen extrusion approach has great potential in advancing tissue repair as a suture, such as for ligament and tendon repair or internal bracing in sports medicine, for improving cosmesis and lifts in plastic surgery, and other surgical indications.

Declaration of Competing Interest

The authors declare that they are or were employees and/or shareholders of Embody Inc. .

Acknowledgments

The work was funded by the Defense Advanced Research Projects Agency (DARPA), grant HR0011-15-9-0006 and 140D0420C0005, AFWERX FA8649-20-9-9080, Commonwealth

Research Commercialization Fund, CP19-034, and Virginia Catalyst (Principal Investigator: Michael Francis for all awards). Multiple authors are or were previously employees of, or students earning degrees at, or interns at Embody Inc. We also thank the Frank Reidy Research Center for Bioelectronics, Dr. Lesley Greene, and John Bedford at the ODU Chemistry Department for their help with chemical analyses. We thank Kevin Francis (<http://kfrancisdesigns.com/>) for designing graphics for this work.

Supplementary materials

Supplementary material associated with this article can be found, in the online version, at [doi:10.1016/j.actbio.2021.04.028](https://doi.org/10.1016/j.actbio.2021.04.028).

References

- [1] A. Ratcliffe, S.S. Ratcliffe, D.L. Butler, N.A. Dymont, P.J. Cagle, E.L. Flatow, C.S. Proctor, Scaffolds for tendon and ligament repair and regeneration, *Ann. Biomed. Eng.* 43 (2015) 819–831, doi:10.1007/s10439-015-1263-1.
- [2] J.H.-C. Wang, Q. Guo, B. Li, Tendon biomechanics and mechanobiology - a mini-review of basic concepts, *J. Hand Ther.* 25 (2012) 133–141, doi:10.1016/j.jht.2011.07.004.
- [3] G.S. Perrone, B.L. Proffen, A.M. Kiapour, J.T. Sieker, B.C. Fleming, M.M. Murray, Bench-to-bedside: bridge-enhanced anterior cruciate ligament repair, *J. Orthop. Res.* (2017), doi:10.1002/jor.23632.
- [4] G. Yang, B.B. Rothrauff, R.S. Tuan, Tendon and ligament regeneration and repair: clinical relevance and developmental paradigm, *Birth Defects Res. Part C - Embryo Today Rev.* 99 (2013) 203–222, doi:10.1002/bdrc.21041.
- [5] O.H. Sherman, M.B. Banffy, Anterior cruciate ligament reconstruction: which graft is best? *Arthrosc. - J. Arthrosc. Relat. Surg.* 20 (2004) 974–980, doi:10.1016/S0749-8063(04)00842-4.
- [6] D.A. Shaerf, Anterior cruciate ligament reconstruction best practice: a review of graft choice, *World J. Orthop.* 5 (2014) 23, doi:10.5312/wjo.v5.i11.23.
- [7] P.B. Voleti, M.R. Buckley, L.J. Soslowsky, Tendon healing: repair and regeneration, *Annu. Rev. Biomed. Eng.* (2012) <https://doi.org/10.1146/annurev-bioeng-071811-150122>.
- [8] M. Krueger-Franke, C.H. Siebert, S. Scherzer, Surgical treatment of ruptures of the Achilles tendon: a review of long-term results, *Br. J. Sports Med.* 29 (1995) 121–125, doi:10.1136/bjism.29.2.121.
- [9] A. van Sliedregt, J.A. van Loon, J. van der Brink, K. de Groot, C.A. van Blitterswijk, Evaluation of polylactide monomers in an in vitro biocompatibility assay, *Biomaterials* 15 (1994) 251–256, doi:10.1016/0142-9612(94)90047-7.
- [10] M.S. Taylor, A.U. Daniels, K.P. Andriano, J. Heller, Six bioabsorbable polymers: in vitro acute toxicity of accumulated degradation products, *J. Appl. Biomater.* 5 (1994) 151–157, doi:10.1002/jab.770050208.
- [11] Y. Matsusue, S. Hanafusa, T. Yamamuro, Y. Shikinami, Y. Ikada, Tissue reaction of bioabsorbable ultra high strength poly (L-lactide) rod: a long-term study in rabbits, *Clin. Orthop. Relat. Res.* 317 (1995) 246–253.
- [12] M.V. Hogan, Y. Kawakami, C.D. Murawski, F.H. Fu, Tissue engineering of ligaments for reconstructive surgery, *Arthrosc. - J. Arthrosc. Relat. Surg.* 31 (2015) 971–979, doi:10.1016/j.arthro.2014.11.026.
- [13] J. Chen, J. Xu, A. Wang, M. Zheng, Scaffolds for tendon and ligament repair: review of the efficacy of commercial products, *Expert Rev. Med. Devices* 6 (2009) 61–73, doi:10.1586/17434440.6.1.61.
- [14] J.K. Seon, E.K. Song, S.J. Park, Osteoarthritis after anterior cruciate ligament reconstruction using a patellar tendon autograft, *Int. Orthop.* 30 (2006) 94–98, doi:10.1007/s00264-005-0036-0.
- [15] T.O. Smith, K. Postle, F. Penny, I. McNamara, C.J.V. Mann, Is reconstruction the best management strategy for anterior cruciate ligament rupture? A systematic review and meta-analysis comparing anterior cruciate ligament reconstruction versus non-operative treatment, *Knee* 21 (2014) 462–470, doi:10.1016/j.knee.2013.10.009.
- [16] J.R.S. Leiter, R. Gourlay, S. McRae, N. de Korompay, P.B. MacDonald, Long-term follow-up of ACL reconstruction with hamstring autograft, *Knee Surg., Sport. Traumatol. Arthrosc.* 22 (2014) 1061–1069, doi:10.1007/s00167-013-2466-3.
- [17] G. Vunjak-Novakovic, G. Altman, R. Horan, D.L. Kaplan, Tissue engineering of ligaments, *Annu. Rev. Biomed. Eng.* 6 (2004) 131–156, doi:10.1146/annurev.bioeng.6.040803.140037.
- [18] S.L.Y. Woo, K. Hildebrand, N. Watanabe, J.A. Fenwick, C.D. Papageorgiou, J.H.C. Wang, Tissue engineering of ligament and tendon healing, *Clin. Orthop. Relat. Res.* (1999), doi:10.1097/00003086-199910001-00030.
- [19] S.H. Liu, R.S. Yang, R. Al-Shaikh, J.M. Lane, Collagen in tendon, ligament, and bone healing: a current review, *Clin. Orthop. Relat. Res.* (1995) 265–278.
- [20] M. Benjamin, *The Structure of Tendons and Ligaments*, Woodhead Publishing, 2010, doi:10.1533/9781845697792.2.351.
- [21] A. Gigante, E. Cesari, A. Busilacchi, S. Manzotti, K. Kyriakidou, F. Greco, R. Di Primio, M. Mattioli-Belmonte, Collagen I membranes for tendon repair: effect of collagen fiber orientation on cell behavior, *J. Orthop. Res.* 27 (2009) 826–832, doi:10.1002/jor.20812.
- [22] E. Gentleman, A.N. Lay, D.A. Dickerson, E.A. Nauman, G.A. Livesay, K.C. Dee, Mechanical characterization of collagen fibers and scaffolds for tissue engineering, *Biomaterials* 24 (2003) 3805–3813, doi:10.1016/S0142-9612(03)00206-0.
- [23] D. Enea, J. Gwynne, S. Kew, M. Arumugam, J. Shepherd, R. Brooks, S. Ghose, S. Best, R. Cameron, N. Rushton, Collagen fibre implant for tendon and ligament biological augmentation. In vivo study in an ovine model, *Knee Surgery, Sport. Traumatol. Arthrosc.* 21 (2013) 1783–1793, doi:10.1007/s00167-012-2102-7.
- [24] M.M. Murray, K.P. Spindler, E. Abreu, J.A. Muller, A. Nedder, M. Kelly, J. Frino, D. Zurakowski, M. Valenza, B.D. Snyder, S.A. Connolly, Collagen-platelet rich plasma hydrogel enhances primary repair of the porcine anterior cruciate ligament, *J. Orthop. Res.* 25 (2007) 81–91, doi:10.1002/jor.20282.
- [25] C. Van Kampen, S. Arnoczky, P. Parks, E. Hackett, D. Ruehlman, A. Turner, T. Schlegel, Tissue-engineered augmentation of a rotator cuff tendon using a reconstituted collagen scaffold: a histological evaluation in sheep, *Muscles. Ligaments Tendons J.* 3 (2013), doi:10.11138/mltj/2013.3.3.229.
- [26] D.J. Bokor, D. Sonnabend, L. Deady, B. Cass, A. Young, C. Van Kampen, S. Arnoczky, Preliminary investigation of a biological augmentation of rotator cuff repairs using a collagen implant: A 2-year MRI follow-up, *Muscles. Ligaments Tendons J.* 5 (2015) 144–150, doi:10.11138/mltj/2015.5.3.144.
- [27] T.F. Schlegel, J.S. Abrams, B.D. Bushnell, J.L. Brock, C.P. Ho, Radiologic and clinical evaluation of a bioabsorbable collagen implant to treat partial-thickness tears: a prospective multicenter study, *J. Shoulder Elb. Surg.* 27 (2018) 242–251, doi:10.1016/j.jse.2017.08.023.
- [28] Y. Maghdouri-White, N. Sori, S. Petrova, H. Wriggers, N. Kemper, N. Thayer, A. Dasgupta, K. Coughenour, S. Polk, M. Rodriguez, A.A. Bulysheva, M.P. Francis, Biomaterial manufacturing and translational research of an aligned collagen-based electrospun tissue engineered device (TEND) for tendon regeneration, *Manuscr. Submitt.* (2020).
- [29] M. Meyer, Processing of collagen based biomaterials and the resulting materials properties, *Biomed. Eng. Online* 18 (2019) 1–74, doi:10.1186/s12938-019-0647-0.
- [30] C.H. Lee, A. Singla, Y. Lee, Biomedical applications of collagen, *Int. J. Pharm.* 221 (2001) 1–21, doi:10.1016/S0378-5173(01)00691-3.
- [31] C. Meena, S.A. Mengi, S.G. Deshpande, Biomedical and industrial applications of collagen, *Proc. Indian Acad. Sci. Chem. Sci.* 111 (1999) 319–329, doi:10.1007/BF02871912.
- [32] A. Rangaraj, K. Harding, D. Leaper, Role of collagen in wound management, *Wounds UK* 7 (2011) 54–63.
- [33] C.C. Chu, Materials for absorbable and nonabsorbable surgical sutures, *Biotextiles As Med. Implant.* (2013) 275–334, doi:10.1533/9780857095602.2.275.
- [34] G. Watts, Sutures for skin closure, *Lancet* 305 (1975) 581.
- [35] M.H. Kuder, S.B. Pai, H. Sripathi, S. Prabhu, Sutures and suturing techniques in skin closure, *Indian J. Dermatol. Venereol. Leprol.* 75 (2009) 425–434, doi:10.4103/0378-6323.53155.
- [36] A.J. Tsugawa, F.J.M. Verstraete, Suture materials and biomaterials, *Oral Maxillofac. Surg. Dugs Cts* (2012) 69–78, doi:10.1016/B978-0-7020-4618-6.00007-5.
- [37] Y.P. Kato, D.L. Christiansen, R.A. Hahn, S.J. Shieh, J.D. Goldstein, F.H. Silver, Mechanical properties of collagen fibres: a comparison of reconstituted and rat tail tendon fibres, *Biomaterials* 10 (1989) 38–42, doi:10.1016/0142-9612(89)90007-0.
- [38] M.G. Dunn, P.N. Avsarala, J.P. Zawadzky, Optimization of extruded collagen fibers for ACL reconstruction, *J. Biomed. Mater. Res.* 27 (1993) 1545–1552, doi:10.1002/jbm.820271211.
- [39] D.I. Zeugolis, G.R. Paul, G. Attenburrow, Cross-linking of extruded collagen fibers—a biomimetic three-dimensional scaffold for tissue engineering applications, *J. Biomed. Mater. Res. - Part A* 89 (2009) 895–908, doi:10.1002/jbm.a.32031.
- [40] N. Reddy, R. Reddy, Q. Jiang, Crosslinking biopolymers for biomedical applications, *Trends Biotechnol.* 33 (2015) 362–369, doi:10.1016/j.tibtech.2015.03.008.
- [41] T.J. Koob, T.A. Willis, Y.S. Qiu, D.J. Hernandez, Biocompatibility of NG-DA-polymerized collagen fibers. II. Attachment, proliferation, and migration of tendon fibroblasts in vitro, *J. Biomed. Mater. Res.* 56 (2001) 40–48 [https://doi.org/10.1002/1097-4636\(200107\)56:1<40::AID-JBM1066>3.0.CO;2-I](https://doi.org/10.1002/1097-4636(200107)56:1<40::AID-JBM1066>3.0.CO;2-I).
- [42] D. Enea, F. Henson, S. Kew, J. Wardale, A. Getgood, R. Brooks, N. Rushton, Extruded collagen fibres for tissue engineering applications: effect of crosslinking method on mechanical and biological properties, *J. Mater. Sci. Mater. Med.* 22 (2011) 1569–1578, doi:10.1007/s10856-011-4336-1.
- [43] A.B. Caruso, M.G. Dunn, Functional evaluation of collagen fiber scaffolds for ACL reconstruction: cyclic loading in proteolytic enzyme solutions, *J. Biomed. Mater. Res. - Part A* 69 (2004) 164–171, doi:10.1002/jbm.a.20136.
- [44] R.G. Paul, A.J. Bailey, Chemical stabilisation of collagen as a biomimetic, *ScientificWorldJournal* 3 (2003) 138–155, doi:10.1100/tsw.2003.13.
- [45] L.M. Delgado, Y. Bayon, A. Pandit, D.I. Zeugolis, To cross-link or not to cross-link? Cross-linking associated foreign body response of collagen-based devices, *Tissue Eng. Part B Rev.* 21 (2015) 298–313, doi:10.1089/ten.teb.2014.0290.
- [46] R. Vijayaraghavan, B.C. Thompson, D.R. MacFarlane, R. Kumar, M. Surianarayanan, S. Aishwarya, P.K. Sehgal, Biocompatibility of choline salts as crosslinking agents for collagen based biomaterials, *Chem. Commun.* 46 (2010) 294–296, doi:10.1039/b910601d.
- [47] M.G. Haugh, M.J. Jaasma, F.J. O'Brien, The effect of dehydrothermal treatment on the mechanical and structural properties of collagen-GAG scaffolds, *J. Biomed. Mater. Res. - Part A* 89 (2009) 363–369, doi:10.1002/jbm.a.31955.
- [48] I.V. Yannas, A.V. Tobolsky, Cross-linking of gelatine by dehydration, *Nature* 215 (1967) 509–510, doi:10.1038/2155099b.
- [49] Z. Ahmad, J.H. Shepherd, D.V. Shepherd, S. Ghose, S.J. Kew, R.E. Cameron, S.M. Best, R.A. Brooks, J. Wardale, N. Rushton, Effect of 1-ethyl-3-(3-

- dimethylaminopropyl) carbodiimide and N-hydroxysuccinimide concentrations on the mechanical and biological characteristics of cross-linked collagen fibres for tendon repair, *Regen. Biomater.* 2 (2015) 77–85, doi:10.1093/rb/rbv005.
- [50] D.V. Shepherd, J.H. Shepherd, S. Ghose, S.J. Kew, R.E. Cameron, S.M. Best, The process of EDC-NHS cross-linking of reconstituted collagen fibres increases collagen fibrillar order and alignment, *APL Mater.* 3 (2015) 1–13, doi:10.1063/1.4900887.
- [51] S. Elder, J. Clune, J. Walker, P. Gloth, Suitability of EGCG as a means of stabilizing a porcine osteochondral xenograft, *J. Funct. Biomater.* 8 (2017), doi:10.3390/jfb8040043.
- [52] L. Wang, J.P. Stegemann, Glyoxal crosslinking of cell-seeded chitosan/collagen hydrogels for bone regeneration, *Acta Biomater.* 7 (2011) 2410–2417, doi:10.1016/j.actbio.2011.02.029.
- [53] T.J. Koob, D.J. Hernandez, Material properties of polymerized NDGA-collagen composite fibers: development of biologically based tendon constructs, *Biomaterials* 23 (2002) 203–212, doi:10.1016/S0142-9612(01)00096-5.
- [54] A.E. Peters, R. Akhtar, E.J. Comerford, K.T. Bates, Tissue material properties and computational modelling of the human tibiofemoral joint: a critical review, *PeerJ* 6 (2018) e4298, doi:10.7717/peerj.4298.
- [55] F. Noyes, E. Grood, The strength of the anterior cruciate ligament in humans and Rhesus monkeys, *J. Bone Jt. Surg.* 58 (1976) 1074–1082, doi:10.2106/00004623-197658080-00006.
- [56] T.A.L. Wren, S.A. Yerby, G.S. Beaupr e, D.R. Carter, Mechanical properties of the human achilles tendon, *Clin. Biomech.* 16 (2001) 245–251, doi:10.1016/S0268-0033(00)00089-9.
- [57] A.J. Gallagher, A. Ni Anniadh, K. Bruyere, M. Ott nio, H. Xie, M.D. Gilchrist, Dynamic tensile properties of human skin, in: 2012 IRCOB Conf. Proc. - Int. Res. Coun. Biomech. Inj., 2012, pp. 494–502.
- [58] K.G. Cornwell, P. Lei, S.T. Andreadis, G.D. Pins, Crosslinking of discrete self-assembled collagen threads: effects on mechanical strength and cell-matrix interactions, *J. Biomed. Mater. Res. Part A* 80 (2007) 362–371.
- [59] M. Franchi, A. Trir e, M. Quaranta, E. Orsini, V. Ottani, Collagen structure of tendon relates to function, *ScientificWorldJournal* 7 (2007) 404–420, doi:10.1100/tsw.2007.92.
- [60] M.D. Shoulders, R.T. Raines, Collagen structure and stability, *Annu. Rev. Biochem.* 78 (2009) 929–958, doi:10.1146/annurev.biochem.77.032207.120833.
- [61] H. Lodish, A. Berk, S. Zipursky, E. A. Al, *Collagen: the Fibrous Proteins of the Matrix in Molecular Cell Biology*. Section 22.3., 4th ed., W. H. Freeman, New York, 2000.
- [62] N. Wiegand, B. Patczai, D. L orinczy, The role of differential scanning calorimetry in the diagnostics of musculoskeletal diseases, *EC Orthop.* 4 (2017) 164–177.
- [63] J.M. Sanchez-Ruiz, Differential scanning calorimetry of proteins, *Proteins Struct. Funct. Eng. Subcell. Biochem.* (1995) 133–176, doi:10.1007/978-1-4899-1727-0_6.
- [64] W. Ming-Che, G.D. Pins, F.H. Silver, Collagen fibres with improved strength for the repair of soft tissue injuries, *Biomaterials* 15 (1994) 507–512, doi:10.1016/0142-9612(94)90016-7.
- [65] C. Haynl, E. Hofmann, K. Pawar, S. F orster, T. Scheibel, Microfluidics-produced collagen fibers show extraordinary mechanical properties, *Nano Lett.* 16 (2016) 5917–5922, doi:10.1021/acs.nanolett.6b02828.
- [66] A. Yaari, Y. Schilt, C. Tamburu, U. Raviv, O. Shoseyov, Wet spinning and drawing of human recombinant collagen, *ACS Biomater. Sci. Eng.* 2 (2016) 349–360, doi:10.1021/acsbomaterials.5b00461.
- [67] K.G. Cornwell, B.R. Downing, G.D. Pins, Characterizing fibroblast migration on discrete collagen threads for applications in tissue regeneration, *J. Biomed. Mater. Res. - Part A* 71 (2004) 55–62, doi:10.1002/jbm.a.30132.
- [68] N.N. Fathima, B. Madhan, J.R. Rao, B.U. Nair, T. Ramasami, Interaction of aldehydes with collagen: effect on thermal, enzymatic and conformational stability, *Int. J. Biol. Macromol.* 34 (2004) 241–247, doi:10.1016/j.ijbiomac.2004.05.004.
- [69] N. Saeidi, K.P. Karamelek, J.A. Paten, R. Zareian, E. DiMasi, J.W. Ruberti, Molecular crowding of collagen: a pathway to produce highly-organized collagenous structures, *Biomaterials* (2012), doi:10.1016/j.biomaterials.2012.06.041.
- [70] M. Benjamin, E. Kaiser, S. Milz, Structure-function relationships in tendons: a review, *J. Anat.* 212 (2008) 211–228, doi:10.1111/j.1469-7580.2008.00864.x.
- [71] M.A. Glomb, V.M. Monnier, Mechanism of protein modification by glyoxal and glycolaldehyde, reactive intermediates of the Maillard reaction, *J. Biol. Chem.* 270 (1995) 10017–10026, doi:10.1074/jbc.270.17.10017.
- [72] B.D. Ratner, The biocompatibility manifesto: biocompatibility for the twenty-first century, *J. Cardiovasc. Transl. Res.* 4 (2011) 523–527, doi:10.1007/s12265-011-9287-x.
- [73] S. Gordon, P.R. Taylor, Monocyte and macrophage heterogeneity, *Nat. Rev. Immunol.* 5 (2005) 953–964, doi:10.1038/nri1733.
- [74] D.M. Mosser, The many faces of macrophage activation, *J. Leukoc. Biol.* 73 (2003) 209–212, doi:10.1189/jlb.0602325.
- [75] E. Kasner, C.A. Hunter, D. Ph, K. Kariko, D. Ph, Macrophage phenotype and remodeling outcomes in response to biologic scaffolds with and without a cellular component, *Biomaterials* 30 (2009) 1482–1491, doi:10.1016/j.biomaterials.2008.11.040.Macrophage.
- [76] B.N. Brown, R. Londono, S. Tottey, L. Zhang, K.A. Kukla, M.T. Wolf, K.A. Daly, J.E. Reing, S.F. Badylak, Macrophage phenotype as a predictor of constructive remodeling following the implantation of biologically derived surgical mesh materials, *Acta Biomater.* 8 (2012) 978–987, doi:10.1016/j.actbio.2011.11.031.
- [77] C.D. Mills, K. Kincaid, J.M. Alt, M.J. Heilman, A.M. Hill, M-1/M-2 macrophages and the Th1/Th2 paradigm, *J. Immunol.* 164 (2000) 6166–6173, doi:10.4049/jimmunol.164.12.6166.
- [78] F. Porcheray, S. Viaud, A.C. Rimaniol, C. L eone, B. Samah, N. Dereuddre-Bosquet, D. Dormont, G. Gras, Macrophage activation switching: an asset for the resolution of inflammation, *Clin. Exp. Immunol.* 142 (2005) 481–489, doi:10.1111/j.1365-2249.2005.02934.x.
- [79] R.D. Stout, C. Jiang, B. Matta, I. Tietzel, S.K. Watkins, J. Suttles, Macrophages sequentially change their functional phenotype in response to changes in microenvironmental influences, *J. Immunol.* 175 (2005) 342–349, doi:10.4049/jimmunol.175.1.342.
- [80] B.N. Brown, S.F. Badylak, Expanded applications, shifting paradigms and an improved understanding of host-biomaterial interactions, *Acta Biomater.* 9 (2013) 4948–4955, doi:10.1016/j.actbio.2012.10.025.